Ultra Wideband Wireless Positioning Systems

by

Mohammadreza Yavari and Bradford G. Nickerson

Technical Report TR14-230

March 27, 2014

Faculty of Computer Science
University of New Brunswick
Fredericton, N.B. E3B 5A3
Canada

Phone: (506) 453-4566
Fax: (506) 453-3566
E-mail: fcs@unb.ca
http://www.cs.unb.ca

Contents

Chapter 1

Ultra Wide-Band Communication

1.1 Definition of Ultra Wide-Band system

The Federal Communication Commission (FCC) [4] has defined UWB systems as those which have an absolute bandwidth larger than 500 MHZ and f_c larger than 2.5 GHZ, or have a B_{frac} larger than 0.2 for systems with f_c lower than 2.5 GHZ. The f_c is the frequency in which the system has the maximum power density (shown in Figure 1.1) and the frequencies f_H and f_L determine the location where the power spectral density is 10 db below the f_c. B_{frac} is defined as

$$B_{frac} = \frac{B}{f_c} \tag{1.1}$$

where B is the bandwidth of the system.

In terms of High and Low frequencies, we have

$$f_c = \frac{f_H + f_L}{2} \tag{1.2}$$

so

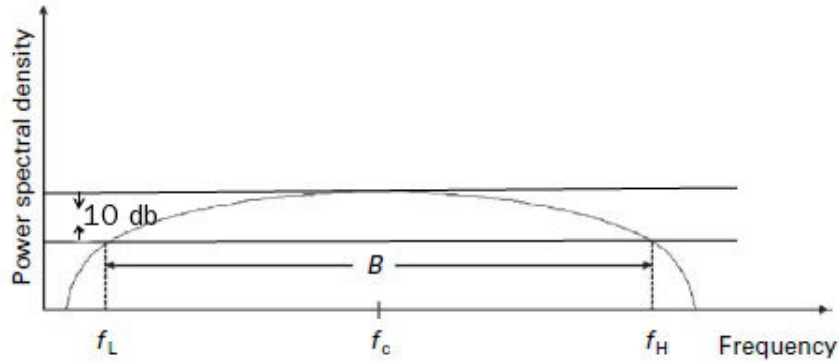$$B_{frac} = \frac{2(f_H - f_L)}{f_H + f_L} \tag{1.3}$$

Figure 1.1: Low, central and high frequencies of an UWB system (from [28]).

1.2 Important features and applications of UWB

The following are some important features of ultra wide-band systems:

- The most important characteristic of UWB is large bandwidth in comparison with prevalent narrow-band systems.

- One result of the large bandwidth of UWB is that due to the inverse relatioship of time and frequency, the life-time of UWB signals is very short. Consequently, the time resolution of UWB signals is high and UWB is a good candidate for positioning systems.

- UWB systems are suitable for high speed communication due to their high bandwidth.

- Another useful property of UWB is that it is permitted to occupy low carrier frequencies, where signals can more easily pass through obstacles.

- UWB signals can be transmitted in base band so there is no need for Intermediate Frequency (IF) multipliers in transceivers. This property can lead to less expensive simpler hardware.

- The high time resolution and short wavelength of UWB signals strengthen it against multipath interference and fading.

- UWB signals' shape is similar to noise so there is a lower chance of eavesdropping.

1.3 Relationship of bandwidth with data rate and power consumption

As indicated by the Shannon-Hartley theorem [23], there is a direct relationship between capacity and bandwidth and an inverse relationship between bandwidth and power con-

sumption. Their theorem states

$$C = B \log_2(1 + \frac{S}{N})$$ (1.4)

where C is the capacity (bits/second), B is the bandwidth, S is the average received signal power over B and N is the average noise over B. We observe that for a specific capacity we consume less power with a larger bandwidth. Secondly, because $\frac{S}{N}$ is under a logarithm, it is easier to increase the capacity by increasing of the bandwidth instead of $\frac{S}{N}$. It is common to refer to $\frac{S}{N}$ as SNR, the Signal to Noise Ratio. Figure 1.2 shows the relationship between the bandwidth and the capacity for five different SNRs.
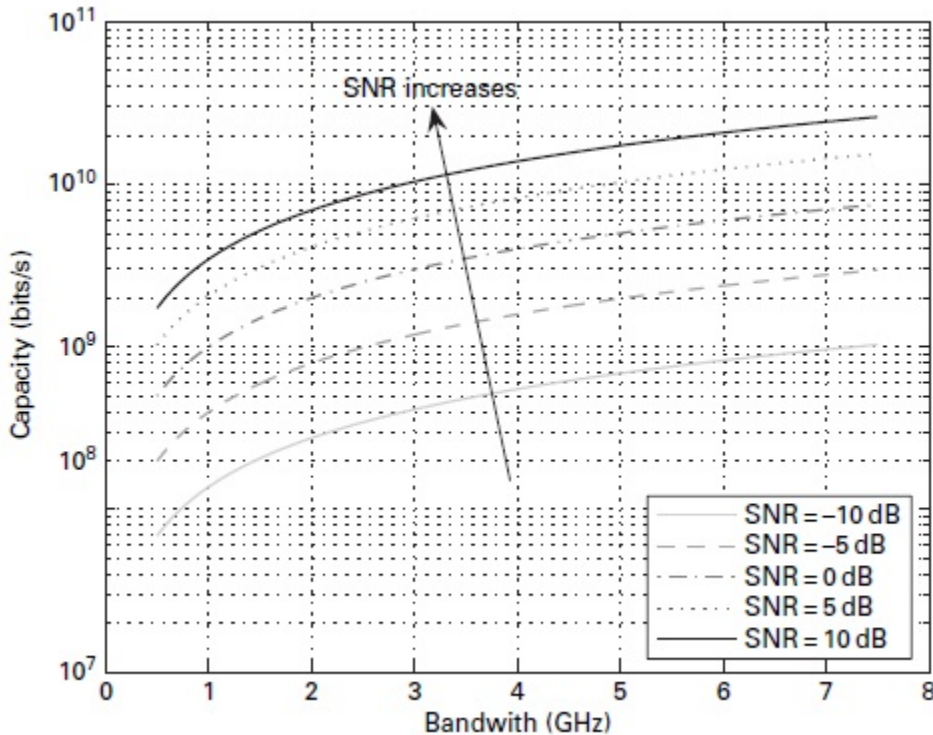
Figure 1.2: Relationship between capacity, bandwidth and SNR (from [28]).

1.4 Impulse Radio (IR) : one method of using UWB

In this method, data is transmitted by low duty UWB signals and information of the symbol is conveyed by position and/or polarity of the signals. Each symbol corresponds to one or more signals. In the following example (Figure 1.3), two consecutive IR signals represent one symbol. The IR signal can occupy one of the chip-intervals (T_c) within a frame (T_f). A time-hopping (TH) code is used for determining the accurate position of a signal in dedicated

time frame to decrease the chance of interference between UWB systems. In the following example, the TH codes for the symbols are $\{2,1\}$, $\{2,3\}$ and $\{1,0\}$ respectively, so the first and second signals are shifted by two and one chip-intervals respectively and so on. In this example the information corresponds to the polarity of signals, so the IR stream represents the binary data "101". This technique is commonly called Binary Phase Shift Keying (BPSK).
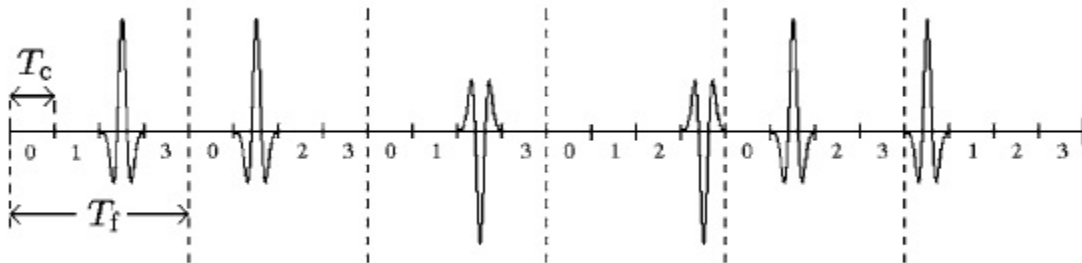
Figure 1.3: IR UWB signals (from [28]).

1.5   Regulation of UWB

Although it is a very useful property of UWB that it has a large bandwidth, this large bandwidth can lead to interference with other narrow band systems. In order to solve this problem some regulations are enforced by several organizations. One of the pioneer organizations in this field is the Federal Communication Commission (FCC). Figure 1.4 demonstrates the FCC's regulation [4] for UWB systems. For UWB radio communication indoors, the FCC part 15.517 requires following equivalent isotropically radiated power (EIRP) limits (1.1). There are many other restrictions for operating of UWB systems in the USA (see [4]). The general approach of all regulations is to restrict the power of signals to avoid collision with other systems. In spite of this restriction, it is an important advantage that UWB is license-free and benefits from co-existence which means that anyone can implement UWB communications without any license in a dedicated range of power in a variety of frequencies.

Table 1.1: Limitation of indoor UWB systems radiating between 960MHZ and 10600MHZ (from [4]).

Frequency in MHz	EIRP in dBm
960-1610	-75.3
1610-1990	-53.3
1990-3100	-51.3
3100-10600	-41.3
Above 10600	-51.3
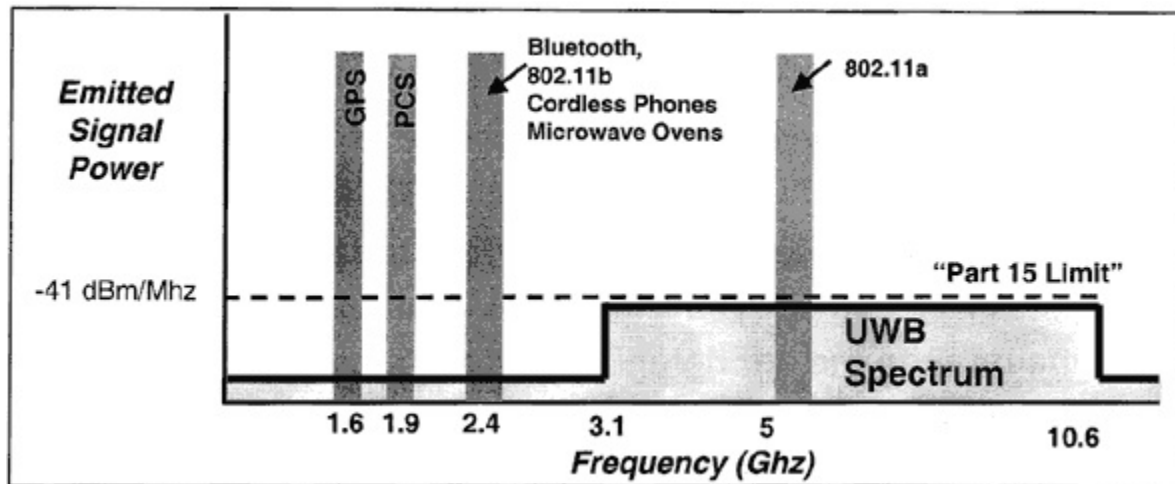
Figure 1.4: FCC regulation for UWB systems (from [22]).

Chapter 2

Position Estimation

There are two approaches for positioning; direct and two-step. In the direct approach the signal is used for positioning itself. In the two-step approach, positioning is based on parameters extracted from the signal but not the signal itself. One consideration is that in the two-step approach, parameters may be extracted from similar but undesired signals; in the direct approach, it is possible to verify the signal's origin. The two-step approach imposes less complexity and is close in performance to the direct approach, so the two step approach is more prevalent in practice and is the focus in this report.
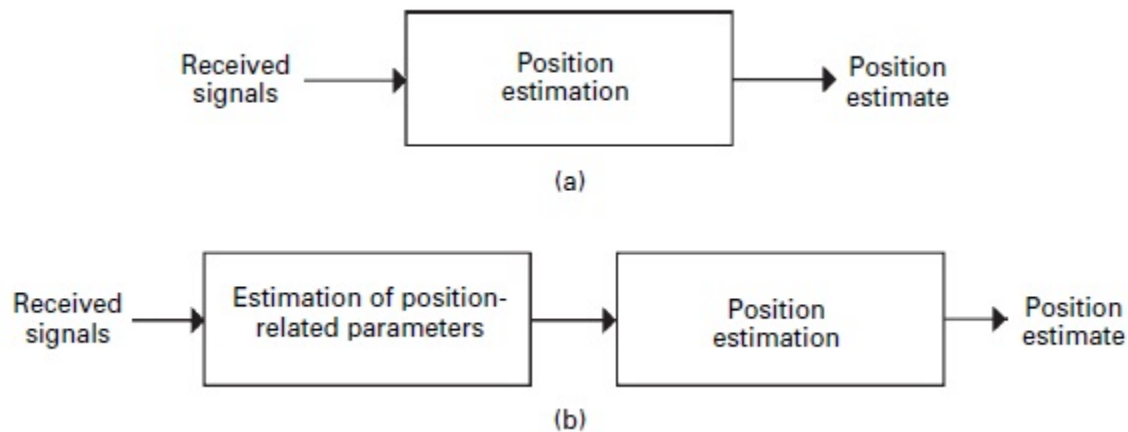
Figure 2.1: (a) The direct approach, and (b) the two-step approach to position estimation (from [28]).

2.1 Signal parameters

2.1.1 Received Signal Strength (RSS)

The strength of a received signal is decreased by path loss (PL) which is proportional to the distance between transmitter and receiver. So we can estimate the range to a target node by measuring RSS. Ideally, the RSS matches $\bar{P}(d)$ in the following :

$$\bar{P}(d) = P_0 - 10n \log_{10}(d/d_0), \tag{2.1}$$

where n is PL exponent, $\bar{P}(d)$ is the received power at distance d and P_0 is the received power at reference distance d_0.

There are two phenomena which affect the amount of PL. The first one is the multi-path phenomenon. Simply, it means that several components of one signal have followed different paths to the receiver, experiencing different amounts of PL. We can overcome this problem by choosing a long enough interval for the following integration

$$P(d) = \frac{1}{T} \int_0^T |r(t)|^2 dt \tag{2.2}$$

where $P(d)$ is the received power and $r(t)$ is the received signal.

The second phenomenon is shadowing or large-scale fading. The main reason for this phenomenon is a changing environment over long distance propagation. The effect of shadowing is modeled with a log-normal random variable:

$$10 \log_{10} P(d) \sim \mathcal{N}(\bar{P}(d), \sigma_{sh}^2) \tag{2.3}$$

where $\bar{P}(d)$ is the average received power and σ_{sh}^2 is the variance of a Gaussian random variable $\mathcal{N}$.

For this model (2.3), the Cramer-Rao lower bound (CRLB) for estimating distance (see [16]) can be expressed as

$$\sqrt{Var\{\hat{d}\}} \geq \frac{ln10}{10} \frac{\sigma_{sh}}{n} d \tag{2.4}$$

where $\hat{d}$ is an unbiased estimate of d. We observe that the bigger the PL exponent n is, the smaller the lower bound is. In addition, a smaller distance d and smaller σ_{sh} gives a smaller lower bound.

In figure 2.2 the minimum standard deviation, $\sigma_{\hat{d}} = \sqrt{Var\{\hat{d}\}}$, of several channels are plotted.

Figure 2.2: (a) Minimum standard deviation of several channels for RSS, with (b) the channel's parameters (from [28]).
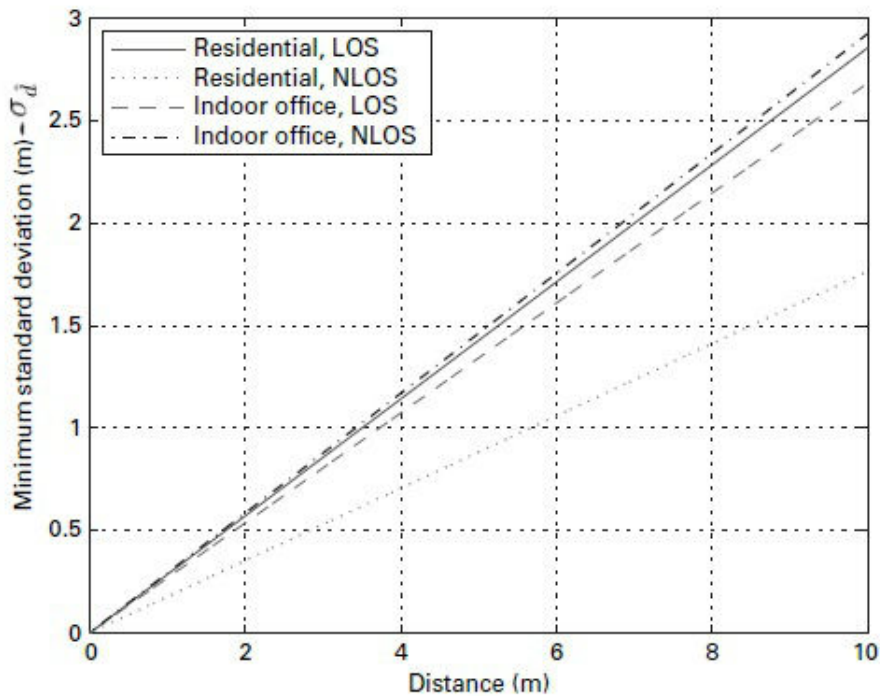
	n	σ_{sh}
Residential LOS	1.79	2.22
Residential NLOS	4.58	3.51
Indoor office LOS	1.63	1.90
Indoor office NLOS	3.07	3.90

(b)

2.1.2 Time Of Arrival (TOA)

Time Of Arrival (TOA) gives us information about the distance between the target node and source node for which the position is known. The target node's position is on a circle of radius $d = c\tau$, for $c =$ speed of light and $\tau =$ time of arrival. The prerequisite of this information is synchronization between the source and target nodes. The received signal at the source node is represented by

$$r(t) = \alpha s(t - \tau) + n(t), \tag{2.5}$$

where τ is the TOA, α is the channel coefficient and $n(t)$ is white Gaussian noise with zero mean and a spectral density of $\mathcal{N}_0/2$ watts per hertz for $\mathcal{N}$ =normal distribution. In order to extract TOA from the received signal, we search for the maximum correlation between shifted versions of the template signal $(s(t - \hat{\tau}))$ and the received signal. The $\hat{\tau}$ which gives the peak correlation provides an estimate of the TOA. For signal model (2.3), the CRLB is

$$\sqrt{Var\{\hat{\tau}\}} \geq \frac{1}{2\sqrt{2}\pi\sqrt{SNR}\beta}, \tag{2.6}$$

where $\hat{\tau}$ is the estimated TOA, SNR $= \alpha^2 E/\mathcal{N}_0$ is the signal to noise ratio, β is the effective signal bandwidth and E is the signal energy. One important property of TOA is that, unlike the RSS, its accuracy is heavily dependent to the bandwidth of the signal. Consequently, UWB systems can reach very precise ranging on the order of a few centimeters. Figure 2.3 shows the effect of SNR and bandwidth on the accuracy of TOA estimation.
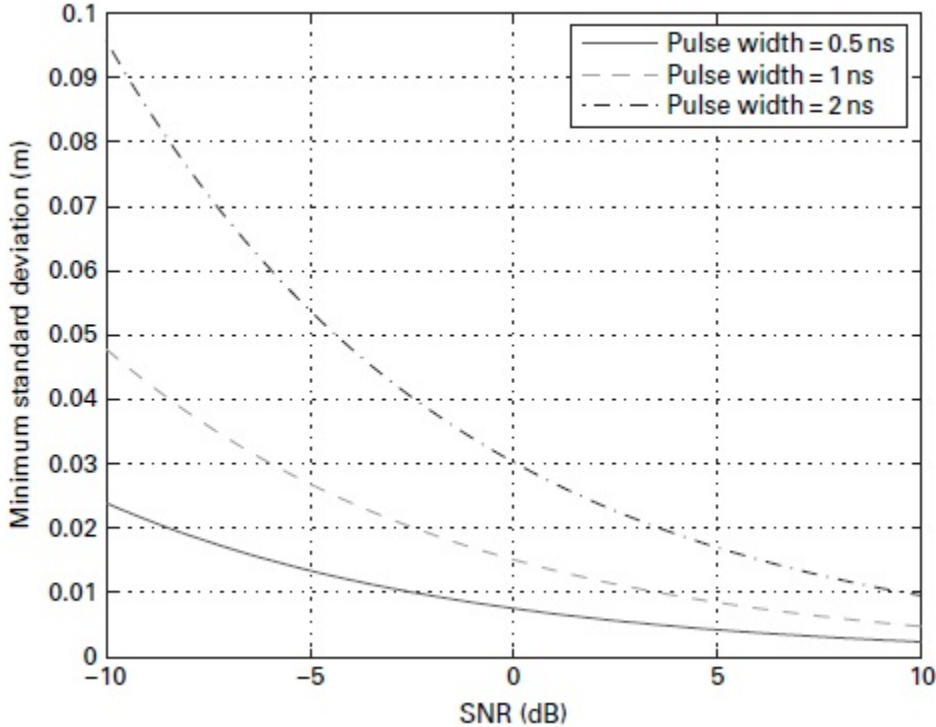

Figure 2.3: Minimum standard deviation of TOA versus SNR for various pulse widths (from [28]).

2.1.3 Time Difference Of Arrival (TDOA)

In this approach, the extracted parameter is the difference between arrival time of transmitted signal (from the target node) to two source nodes. This parameter, by multiplying

TDOA by the speed of light, gives us an uncertainty of the target node's position in the shape of a hyperbola as shown in figure 2.4.
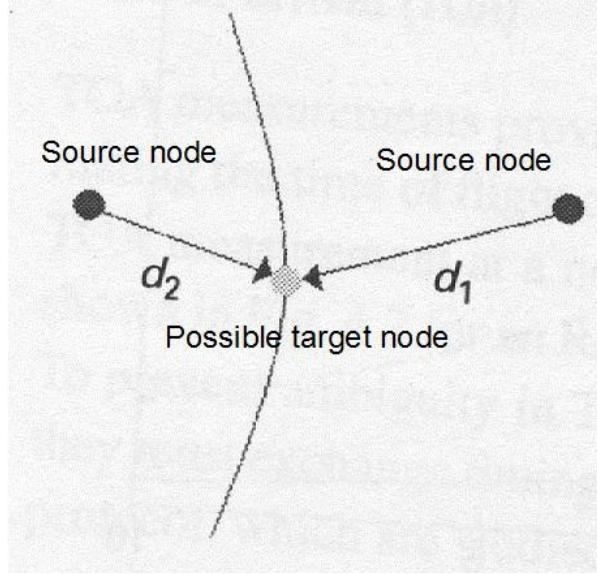
Figure 2.4: The hyperbola indicated by TDOA (from [28]).

The merit of TDOA in comparison with TOA is that there is no need for synchronization between source nodes and the target node. Source nodes however, do need to be synchronized. In the TOA based approach for measuring TDOA, TOA is measured at two source nodes which we call τ_1 and τ_2. As source nodes and target node are not synchronized, there is a time offset in τ_1 and τ_2. Since sources are synchronized with themselves, this offset is equal in both measurements. Consequently, we can measure the TDOA as

$$\tau_{TDOA} = \tau_1 - \tau_2, \tag{2.7}$$

where τ_{TDOA} is the estimation of TDOA. In this approach there is the same effect of bandwidth as in TOA measurements.

The second approach to measure the TDOA is using cross-correlation between two received signals. We know that there is some amount of offset between received signals so the cross-correlation will reach a maximum when one of the signals is shifted with correct offset. The cross-correlation equation is

$$\phi_{1,2}(\tau) = \frac{1}{T} \int_0^T r_1(t) r_2(t + \tau) dt \tag{2.8}$$

where $r_1(t)$ and $r_2(t)$ are the received signals and T is the observation interval. Then we estimate TDOA, $\hat{\tau}_{TDOA}$ by

$$\hat{\tau}_{TDOA} = \arg\max_{\tau} |\phi_{1,2}(\tau)| \tag{2.9}$$

where

$$\arg\max_{x} f(x) := \{x | \forall y : f(y) \leq f(x)\} \tag{2.10}$$

The cross-correlation approach works well for white noise and single path channels but in the case of multi-path channel or colored noise its performance decreases significantly.

2.1.4 Angle of arrival (AOA)

AOA is another parameter of the signal which includes information about the position of the target node. In this case we estimate the angle, ψ, between an array of antennas and the target node regards to the delay between arrival of the signal to antennas. AOA gives us an uncertainty region with the shape of a line, as depicted in figure 2.5.
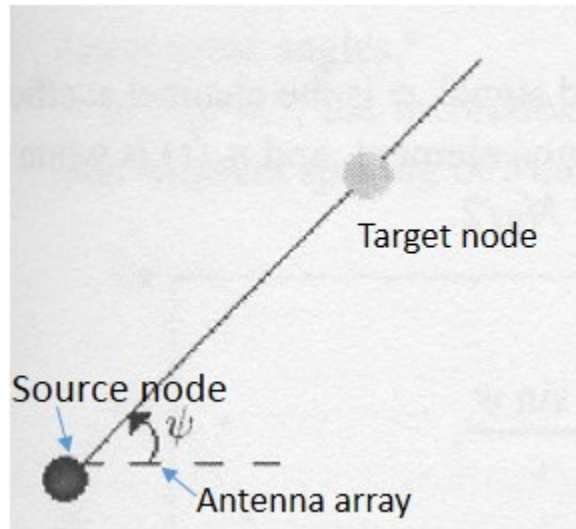
Figure 2.5: The angle between an antenna array and transmitting target node (adapted from [28]).

The antenna array may be in different arrangements; the simplest one is the uniform linear array (ULA) as shown in Figure 2.6. In the case of ULA, the delay between arrival of the signals to the consecutive antennas is given by

$$\tau = \frac{l \sin \psi}{c} \tag{2.11}$$

where τ is the delay, l is the distance between consequent antennas, ψ is the AOA and c is the speed of light.
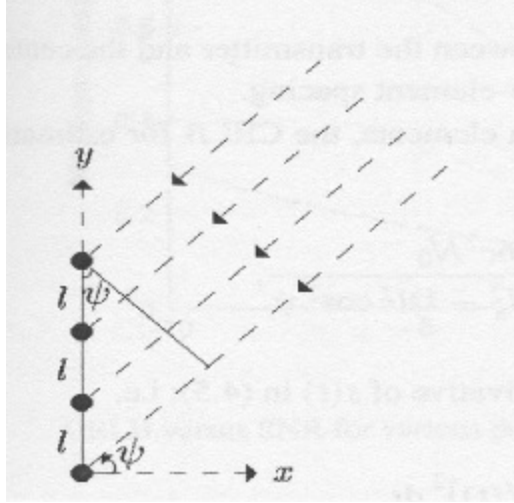
Figure 2.6: Uniform linear array of antennas (from [28]).

In order to measure the accuracy of the AOA approach, we formulate the received signal to each of N_a antennas by

$$r_i(t) = \alpha s(t - \tau_i) + n_i(t) \tag{2.12}$$

where α is the coefficient of the channel, τ_i is the delay for the ith antenna and $n_i(t)$ is a white Gaussian noise with zero mean and spectral density of $\mathcal{N}_0/2$. We can express the delay of the signal received by the ith antenna as

$$\tau_i \approx \frac{d}{c} + \frac{l_i \sin(\psi)}{c} \tag{2.13}$$

where

$$l_i = l(\frac{N_a + 1}{2} - i), \tag{2.14}$$

and d is the distance between the target node and the center of the antenna array.

The CRLB for estimating ψ is

$$\sqrt{Var\{\hat{\psi}\}} \geq \frac{\sqrt{3}c}{\sqrt{2}\pi\sqrt{SNR}\beta\sqrt{N_a(N_a^2 - 1)}l \cos\psi} \tag{2.15}$$

We observe that the accuracy of the AOA method is dependent on SNR, β, N_a, l and ψ. Our main interest is the effect of bandwidth on the accuracy since we can use signals with very small pulse time in the UWB systems. Figure 2.7 depicts the effect of pulse width and SNR on CRLB for angle of arrival. In this case, other parameters are assumed to be fixed.

14
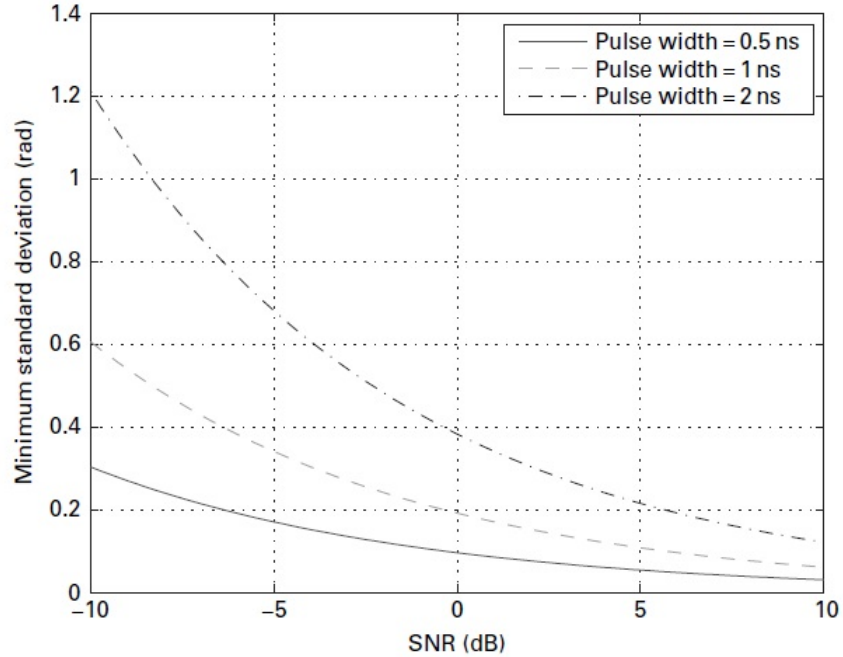
Figure 2.7: CRLB for angle of arrival versus SNR for several pulse-widths (from [28]).

We observe that increasing bandwidth (decreasing pulse-width) has a significant effect on the accuracy. In other words, with high bandwidth we can gain high accuracy even with low SNR. Consequently, UWB is a very good candidate for the AOA approach.

In figure 2.8 the effect of AOA on its estimation accuracy is depicted. We observe that even for wide-band signals the accuracy will be decreased dramatically for angles bigger than 1 rad (57 degrees) or smaller than 1 rad. As one suggestion, we can use several antenna arrays and weight the estimation of each array by the inverse of estimated angle.
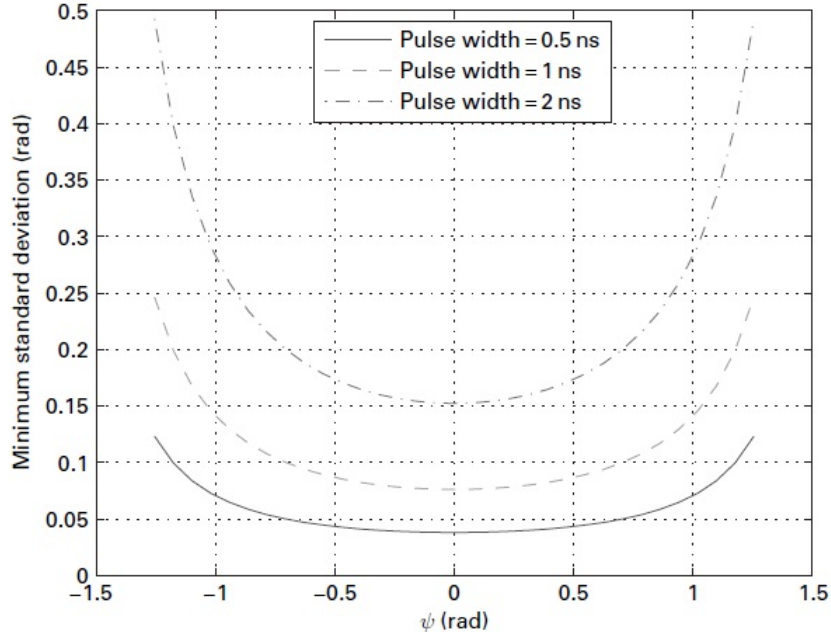
Figure 2.8: CRLB for AOA versus ψ (AOA) for several pulse-widths (from [28]).

2.2 Position estimation using parameters

In this section we discuss methods of position estimation based on the parameters we cited in the last section. There are two main categories of positioning methods.The mapping category uses a calibration table which includes any of the above measurements corresponding to known positions. This calibration table is produced prior to the positioning in a training phase. One important consideration in mapping category methods is updating the calibration table of known positions which is challenging, especially in outdoor positioning systems. Consequently, mapping category methods are not prevalent in outdoor applications. In this report, our focus is on the non-mapping category which uses parameters extracted directly from the signal instead of a pre-computed calibration table. The mapping category of positioning approaches has two sub-categories; geometric approaches and statistical approaches, which are discussed separately in the next two sections.

2.2.1 Geometric approach

In the last section we observed that each of the signal parameters gives us an uncertainty of the target node's position; for example the RSS and TOA give us an uncertainty in the shape of a circle while the AOA gives us an uncertainty in the shape of a line. In the geometric approach, the position of the target node is determined by the intersection of uncertainty regions computed on several source nodes. For example, in the case of RSS or TOA, we need

16

to know the distance between target node and three source nodes with known position, d_i, as shown in Figure 2.9
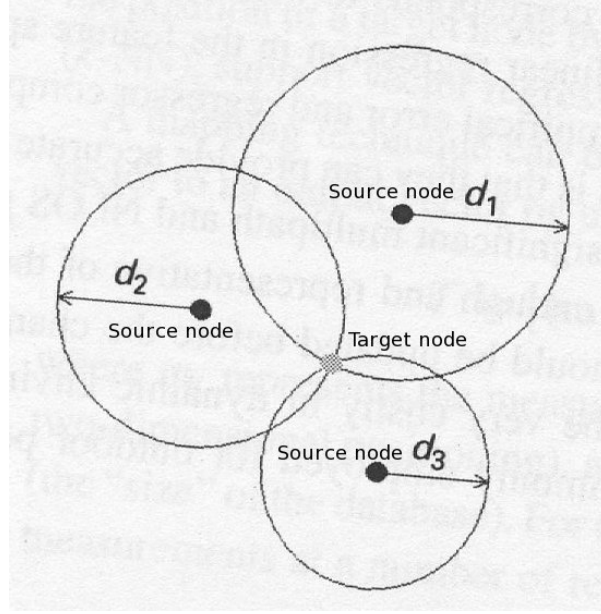
Figure 2.9: The distance between source nodes and the target node is computed by RSS or TOA. The target node's position is estimated by intersection of three circles (from [28]).

We can compute the unique intersection of resulting circles which is our estimate for the position of the target node. The following equation (from [28]), computes the position of the target node, (x, y), based on determined distance of the target node, d_i, from the source nodes with the position (x_i, y_i)

$$x = \frac{(y_2 - y_1)\gamma_1 + (y_2 - y_3)\gamma_2}{2[(x_2 - x_3)(y_2 - y_1) + (x_1 - x_2)(y_2 - y_3)]}, \qquad (2.16)$$

$$y = \frac{(x_2 - x_1)\gamma_1 + (x_2 - x_3)\gamma_2}{2[(x_2 - x_1)(y_2 - y_3) + (x_2 - x_3)(y_1 - y_2)]}, \qquad (2.17)$$

where

$$\gamma_1 = x_2^2 - x_3^2 + y_2^2 - y_3^2 + d_3^2 - d_2^2, \qquad (2.18)$$

$$\gamma_2 = x_1^2 - x_2^2 + y_1^2 - y_2^2 + d_2^2 - d_1^2. \qquad (2.19)$$

The equation (2.16) is derived by solving these three equations (from [28]) jointly

$$d_i = \sqrt{(x_i - x)^2 + (y_i - y)^2}, i = 1, 2, 3. \qquad (2.20)$$

Using the AOA approach, we need only two source nodes (antenna arrays) to estimate the position of the target node. As depicted in Figure 2.10, each measured AOA gives us an uncertainty in the shape of a line; so, we can estimate the target node's position as the intersection of these two lines.
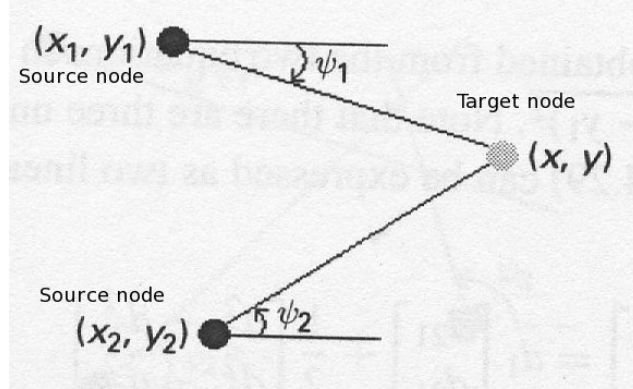
Figure 2.10: The angle, ψ_i, between each source node and the target node limits the position of the target node to a line (from [28]).

Each line gives an equation like

$$\tan \psi = \frac{y - y_i}{x - x_i}, i = 1, 2 \tag{2.21}$$

Solving the two equations jointly, we have (from [28])

$$x = \frac{x_2 \tan \psi_2 - x_1 \tan \psi_1 + y_1 - y_2}{\tan \psi_2 - \tan \psi_1} \tag{2.22}$$

$$y = \frac{(x_2 - x_1) \tan \psi_2 \tan \psi_1 + y_1 \tan \psi_2 - y_2 \tan \psi_1}{\tan \psi_2 - \tan \psi_1}. \tag{2.23}$$

In the case of TDOA, we need three source nodes with known positions to obtain two TDOAs. As explained in the previous section, TDOA is time difference of arrival of transmitted signals from the target node, between two source nodes. One TDOA gives us an uncertainty region in the shape of a hyperbola.
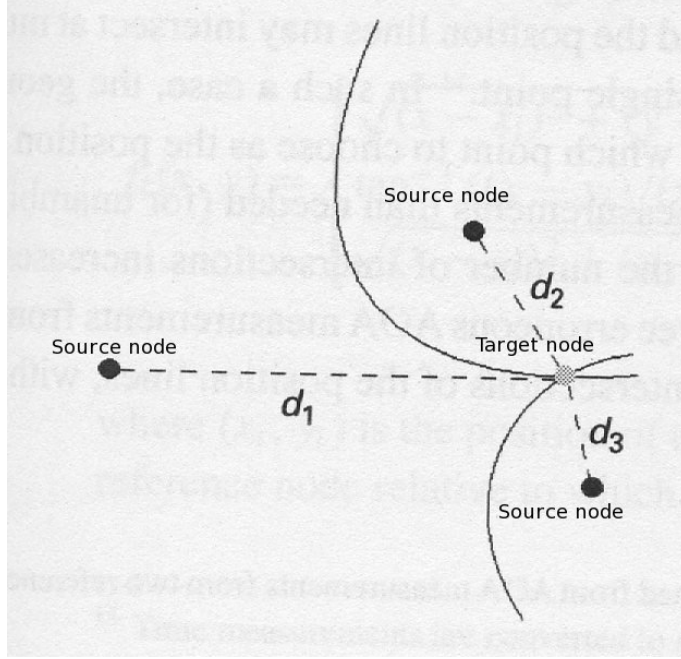
Figure 2.11: Each TDOA determines a hyperbola. The position of the target node is estimated by intersection of these two hyperbolae (from [28]).

The hyperbola region is described by the following equation :

$$d_{i1} = d_i - d_1 = \sqrt{(x - x_i)^2 - (y - y_i)^2} - \sqrt{(x - x_1)^2 + (y - y_1)^2}, \text{for } i = 2, 3, \qquad (2.24)$$

where

$$d_1 = \sqrt{(x - x_1)^2 - (y - y_1)^2}. \qquad (2.25)$$

The position of the target node is estimated by solving the two equations of (2.24) jointly. For detailed solution for the TDOA case see [21].

In addition to these cases, there are some combined approaches. In these combined approaches several parameters are extracted and the position of the target node is estimated by the intersection of different provided uncertainty shapes. As two examples TDOA/AOA [5] and TOA/TDOA [19] are implemented. Figure 2.12 shows the TOA/AOA approach. In this case we need only one source node with known position which has the ability of measuring both TOA and AOA parameters.
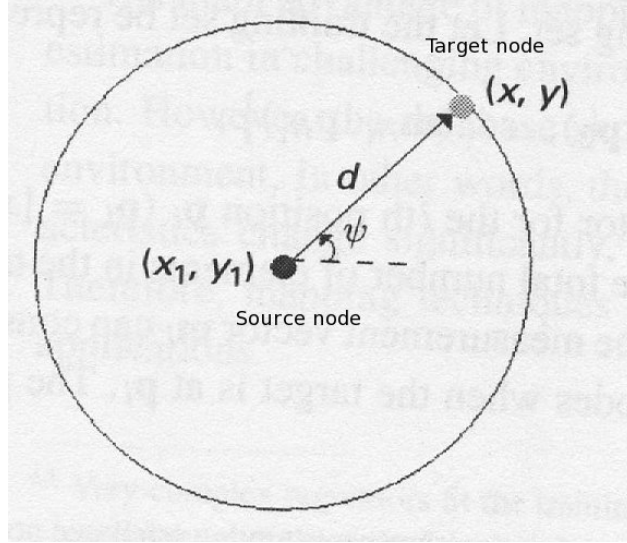
Figure 2.12: The position of target node is determined by the intersection of a line (AOA measurement) and a circle (TOA measurement) (from [28]).

In this case we can estimate the position of the target node as

$$x = x_1 + d \cos \psi, y = y_1 + d \sin \psi, \tag{2.26}$$

where ψ is the AOA and d is the TOA.

All of the positioning approaches mentioned in this section were based on an assumption that there is no noise in measurements; so, uncertainty regions intersect in just one point. In practice, we have always some amount of noise in our measurements. Thus, the result of several measurements is more than one intersection. Figure 2.13 shows a result of noisy AOA measurements. Since measured angles are not accurate, the resulting lines intersect in three different points. Geometric approaches don't give us any idea about estimating the target node's position in such cases. Consequently, we should consider statistical approaches.
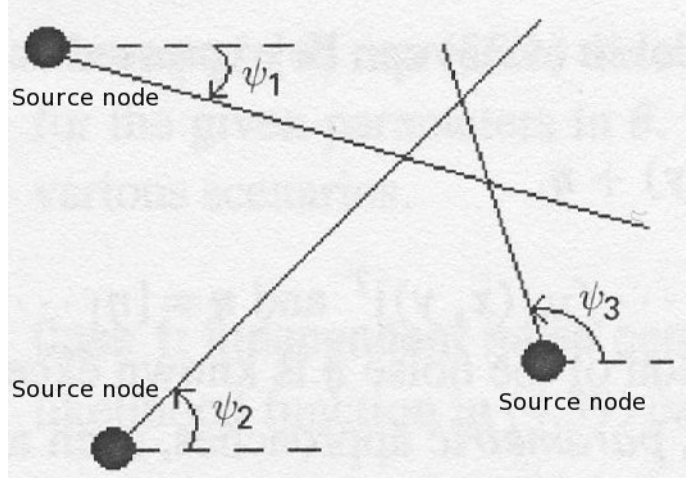
Figure 2.13: Three AOA uncertainty regions don't have a unique intersection, due to the noise in measurements (from [28]).

2.2.2 Statistical approach

Since geometric approaches cannot cope with practical noisy environments, usually statistical approaches are used in practice. In this noisy framework, we define a model (adapted from [28]) for noisy measurements as

$$z = f(x, y) + \eta, \tag{2.27}$$

where z is the result of a noisy measurement, $f(x, y)$ is the true value of this measurement which is a function of target node's position and η is the noise of this measurement. For the techniques discussed in this section, $f(x, y)$ is as follows (adapted from [28]) :

$$f(x, y) = \begin{cases} \sqrt{(x - x_s)^2 + (y - y_s)^2} & TOA/RSS \\ \arctan((y - y_s)/(x - y_s)) & AOA \\ \sqrt{(x - x_s)^2 + (y - y_s)^2} - \sqrt{(x - x_{cs})^2 + (y - y_{cs})^2} & TDOA \end{cases} \tag{2.28}$$

where (x_s, y_s) is the known position of the source node, and (x_{cs}, y_{cs}) is the position of the common source node for the TDOA technique. In vector-space notation, the cited model is changed to (from [28])

$$\mathbf{z} = \mathbf{f}(x, y) + \boldsymbol{\eta}, \tag{2.29}$$

where $\mathbf{z} = [z_1...z_{N_m}]^T$, $\mathbf{f}(x, y) = [f_1(x, y)....f_{N_m}(x, y)]^T$ and $\boldsymbol{\eta} = [\eta_1...\eta_{N_m}]^T$. N_m is equal to the number of source nodes in TOA, RSS and AOA approaches, and one less than the number of source nodes in the TDOA approach. Assume that the noise which affects our measurement is known except for a set of parameters, $\boldsymbol{\lambda}$. So, we have a vector of unknown parameters, $\boldsymbol{\theta}$, as (from [28])

$$\boldsymbol{\theta} = [xy\boldsymbol{\lambda}^T]^T \tag{2.30}$$

where (x, y) is the position of the target node. In such problems, we can use parametric approaches to estimate the true value of $\boldsymbol{\theta}$. Two prevalent parametric approaches are Bayesian and Maximum-Likelihood (ML) [2]. The Bayesian approach is useful in the case that some prior information about $\boldsymbol{\theta}$ is available. In this report, we assume no such prior information, so, we focus on the ML approach. The ML approach finds $\boldsymbol{\theta}$ which gives the maximum probability for the observations. Formally, we can define $\boldsymbol{\theta}$ estimated by the ML, $\hat{\boldsymbol{\theta}}_{ML}$, as

$$\hat{\boldsymbol{\theta}}_{ML} = \arg\max_{\boldsymbol{\theta}} p(\mathbf{z}|\boldsymbol{\theta}). \tag{2.31}$$

Since the function $f(x, y)$ is deterministic, we can express the likelihood function, $p(\mathbf{z}|\boldsymbol{\theta})$ as

$$p(\mathbf{z}|\boldsymbol{\theta}) = p_{\boldsymbol{\eta}}(\mathbf{z} - \mathbf{f}(x, y)|\boldsymbol{\theta}), \tag{2.32}$$

where $p(.|\boldsymbol{\theta})$ is the conditional probability density function of the noise for a given parameter vector $\boldsymbol{\theta}$.

Positioning in the presence of independent noise

In the case of independent noise for all measurements we can express equation (2.32) as

$$p(\mathbf{z}|\boldsymbol{\theta}) = \prod_{i=1}^{N_m} p_{\eta_i}(z_i - f_i(x, y)|\boldsymbol{\theta}) \tag{2.33}$$

where z_i is the ith measurement, $f_i(x, y)$ is the true value of the ith measurement and the p_{η_i} is the conditional probability density function of the ith measurement. The independent noise assumption is reasonable for the AOA, TOA and RSS approaches. However, in the case of TDOA, we have correlated noise for several source nodes' measurements due to the presence of the common source node. For systems working under LOS conditions, the majority of the noise is thermal noise. We can model the noise of these environments as a Gaussian zero mean random variable as

$$p_{\eta_i}(u) = \frac{1}{\sqrt{2\pi}\sigma_i} exp(-\frac{u^2}{2\sigma_i^2}). \tag{2.34}$$

The unknown variables vector $\boldsymbol{\theta}$, reduces to $[x, y]^T$. Then the likelihood function in (2.33) is expressed as

$$p(\mathbf{z}|\boldsymbol{\theta}) = \frac{1}{2\pi^{N_m/2} \prod_{i=1}^{N_m} \sigma_i} exp\left(-\sum_{i=1}^{N_m} \frac{(z_i - f_i(x, y))^2}{2\sigma_i^2}\right). \tag{2.35}$$

With this expression of the $p(\mathbf{z}|\boldsymbol{\theta})$, the ML estimator for (2.31) is calculated by (from [28])

$$\hat{\boldsymbol{\theta}}_{ML} = \arg\min_{[x,y]^T} \left(\sum_{i=1}^{N_m} \frac{(z_i - f_i(x, y))^2}{\sigma_i^2}\right) \tag{2.36}$$

22

where

$$\underset{(x,y)}{\arg\min} f(x,y) := \{(x,y) | \forall(w,z) : f(w,z) \geq f(x,y)\}. \qquad (2.37)$$

Equation (2.36) is a commonly used non-linear least squares (NLS) estimator [24]. In the case of sufficiently large effective bandwidth and SNR the standard deviation of thermal noise, σ_i^2, is given by $\frac{1}{8\pi^2\beta^2 SNR}$, where β is the effective bandwidth of the signal and SNR is the signal to noise ratio[18]. We observe that the variance of the noise in each measurement weights the measurement in an inverse manner, which matches our intuition that stronger noise implies less accurate measurement. Several approaches are cited in literature to solve (2.36) equation including gradient descent algorithms and linearization techniques using Taylor expansion[12][15].

Positioning in the presence of dependent noise

Using TDOA approach we have dependent noise, since there is a common source node in all TDOA measurements. In this case equation (2.33) is not consistent. We use multivariate normal random variable to model the correlated noise of TDOA measurements. A random vector $\mathbf{x} = (\mathbf{X_1}, \mathbf{X_2}, ..., \mathbf{X_k})$ is a multivariate normal random variable if any linear combination of its components, $Y = a_1 X_1 + a_2 X_2 + ... + a_k X_k$, is a normal random variable [9]. The following notation is used for a k-dimensional multivariate normal random variable

$$\mathbf{x} \sim \mathcal{N}_k(\boldsymbol{\mu}, \boldsymbol{\Sigma}) \qquad (2.38)$$

where $\boldsymbol{\mu}$ is a k-dimensional vector of univariate normal random variables' mean as

$$\boldsymbol{\mu} = [E[X_1], E[X_2], ..., E[X_k]] \qquad (2.39)$$

and $\boldsymbol{\Sigma}$ is a k by k matrix of covariance between each pair of univariate normal random variables as

$$\boldsymbol{\Sigma}[i,j] = Cov[X_i, X_j] \text{ for } i = 1, 2, 3, ..., k \ j = 1, 2, 3, ..., k \qquad (2.40)$$

Modeling the correlated noise of TDOA measurement by multivaiate normal random variable, the general form of likelihood function (2.32) is expressed as (from [28])

$$p(\boldsymbol{z}|\boldsymbol{\theta}) = \frac{1}{(2\pi)^{N_m/2}|\boldsymbol{\Sigma}|^{1/2}} exp\left\{-\frac{1}{2}(\mathbf{z} - \mathbf{f}(x,y) - \boldsymbol{\mu})^T \boldsymbol{\Sigma}^{-1}(\mathbf{z} - \mathbf{f}(x,y) - \boldsymbol{\mu})\right\} \qquad (2.41)$$

Then, the ML estimation of the $\boldsymbol{\theta}$ is expressed by

$$\hat{\boldsymbol{\theta}}_{ML} = \underset{\boldsymbol{\theta}}{\arg\min}\left\{(\mathbf{z} - \mathbf{f}(x,y) - \boldsymbol{\mu})^T \Sigma^{-1}(\mathbf{z} - \mathbf{f}(x,y) - \boldsymbol{\mu}) + \log|\boldsymbol{\Sigma}|\right\} \qquad (2.42)$$

Where unknown variables vector, $\boldsymbol{\theta}$, includes the position of the target node and unknown parameters of $\boldsymbol{\Sigma}$ and $\boldsymbol{\mu}$. If the average of noise is zero and the covariance matrix of correlated

noise is known, the $\boldsymbol{\theta}$ just includes the target node's position, [x,y], and the ML estimation is expressed by

$$\hat{\boldsymbol{\theta}}_{ML} = \arg\min_{[x,y]^T}(\mathbf{z} - \mathbf{f}(x,y))^T \boldsymbol{\Sigma}^{-1}(\mathbf{z} - \mathbf{f}(x,y)) \tag{2.43}$$

which is called the weighted LS (WLS) solution [12].

We know that the majority of the noise in our measurements is the thermal noise and Formerly, we modeled thermal noise with a zero mean normal random variable. In addition we mentioned an equation for determining the standard deviation of this normal random variable by the SNR and the effective bandwidth of the recieved signal. Then we determine the covariance matrix of the noise in a TDOA measurement system which is based on (N_m+1) TOA measurements as (from [28])

$$\boldsymbol{\Sigma} = \begin{pmatrix} \sigma_{cs}^2 + \sigma_1^2 & \sigma_{cs}^2 & \cdots & \sigma_{cs}^2 \\ \sigma_{cs}^2 & \sigma_{cs}^2 + \sigma_2^2 & \cdots & \sigma_{cs}^2 \\ \vdots & \vdots & \ddots & \vdots \\ \sigma_{cs}^2 & \sigma_{cs}^2 & \cdots & \sigma_{cs}^2 + \sigma_{N_m}^2 \end{pmatrix} \tag{2.44}$$

where σ_i is the variance of the thermal noise in the ith TOA measurement for $i = 1, 2, ..., N_m$ and σ_{cs} is the variance of the thermal noise in the TOA measurement performed by the common source node.

Positioning in the case of non line of sight (NLOS) propagation

In the most practical systems there are some obstacles between the target node and source nodes. Therefore, signals transmitted by the target node have to pass a longer indirect path to reach the source node. Figure 2.14 depicts the difference between NLOS propagation and LOS propagation.

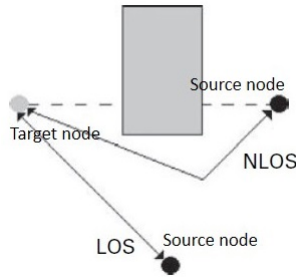Figure 2.14: NLOS and LOS propagations (from [28]).

It is observable that NLOS propagation acts as a noise source regarding cited signal parameters such as TOA, RSS and AOA; we call this noise NLOS noise. For example, the TOA of the signal increases since it has to follow a longer path and the time of arrival is affected by a positive noise. Due to NLOS propagation, the noise model in equation (2.34) is

not accurate for NLOS cases. The NLOS noise is commonly modeled by a Gamma probability distribution. The NLOS noise dominates the background noise modeled by equation (2.34). In the next section we discuss an approach for mitigating NLOS noise by using a Kalman filter.

2.2.3   Evaluating estimation by mean square error(MSE)

When an unknown vector, $\boldsymbol{\theta}$, is estimated as $\hat{\theta}$, the accuracy of the estimation is commonly evaluated by MSE as

$$MSE = E\{(\hat{\boldsymbol{\theta}} - \boldsymbol{\theta})^2\} \tag{2.45}$$

The CramrRao lower bound (CRLB) sets a lower bound for the MSE which is called minimum mean square error (MMSE). Generally, when $\hat{\boldsymbol{\theta}}$ is an estimation of the $\boldsymbol{\theta}$ based on a set of measurements, $\mathbf{z}$, the CRLB sets the lower bound of covariance matrix of estimation as:

$$E\left\{(\hat{\boldsymbol{\theta}} - \boldsymbol{\theta})(\hat{\boldsymbol{\theta}} - \boldsymbol{\theta})^T\right\} \geq \mathbf{I_{\theta}}^{-1} \tag{2.46}$$

where $\mathbf{I}_\theta$ is the Fisher information matrix (FIM) represented as

$$\mathbf{I_{\theta}} = E\left\{\frac{\partial \log p(\mathbf{z}|\boldsymbol{\theta})}{\partial \boldsymbol{\theta}}\left(\frac{\partial \log p(\mathbf{z}|\boldsymbol{\theta})}{\partial \boldsymbol{\theta}}^T\right)\right\} \tag{2.47}$$

In order to obtain a lower bound for the MSE, we represent MSE as the trace (sum of diagonal entries) of the covariance matrix of estimation. Then CRLB obtains MMSE as

$$MSE = E\{(\hat{\boldsymbol{\theta}} - \boldsymbol{\theta})^2\} = trace\left[E\left\{(\hat{\boldsymbol{\theta}} - \boldsymbol{\theta})(\hat{\boldsymbol{\theta}} - \boldsymbol{\theta})^T\right\}\right] \geq trace\left[\mathbf{I_{\theta}}^{-1}\right] = MMSE \tag{2.48}$$

Here we explain the above equation with an example (from [28]) of a positioning system based on the TOA approach. Consider there are N_m source nodes in the system, N_L of which are in LOS and others are in NLOS condition. Without loss of generality, assume that source nodes from 1 to N_L are LOS nodes. It is shown in [17] that the MMSE for such a system, in the absence of statistical information about NLOS noise, is expressed as

$$MMSE_{TOA} = \frac{c^2 \sum\limits_{i=1}^{N_L} SNR_i}{8\pi^2\beta^2 \sum\limits_{i=1}^{N_L} \sum\limits_{j=1}^{i-1} SNR_i SNR_j \sin^2(\psi_i - \psi_j)} \tag{2.49}$$

where SNR_i is the signal to noise ratio of the ith source node, c is the speed of light, β is the effective bandwidth and ψ_i is the angle between the ith source node and the target node. Angle ψ_i is computed as

$$\psi_i = \arctan(\frac{(y - y_i)}{(x - x_i)}) \tag{2.50}$$

where (x, y) is the position of the target node and (x_i, y_i) is the position of the ith source node. It is observable in equation (2.16) that in the absence of statistical information about the NLOS noise, the lower bound of accuracy is independent of the source nodes in a NLOS position. In addition, this equation shows the positive effect of larger bandwidth and SNR on the accuracy of the positioning. In the example depicted in figure 2.15 there are six source nodes positioned on a circle around the target node with equal distances.
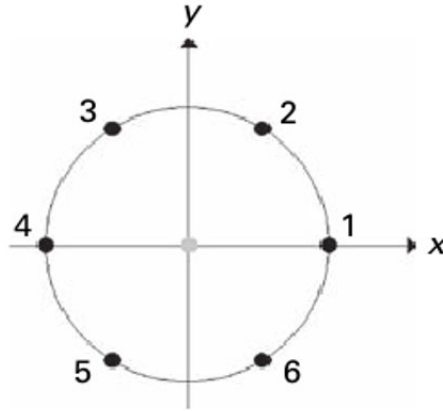
Figure 2.15: Example positioning scenario (from [28]).

Figure 2.16 depicts the root mean square error (RMSE) (which is the square root of the MMSE) for different SNRs and three different values N_L for the number of the LOS source nodes. It is observable that the SNR and number of LOS source nodes have a direct affect on the accuracy of the system. In addition we conclude that when a low SNR signal exists, it is much more important to have more LOS nodes.
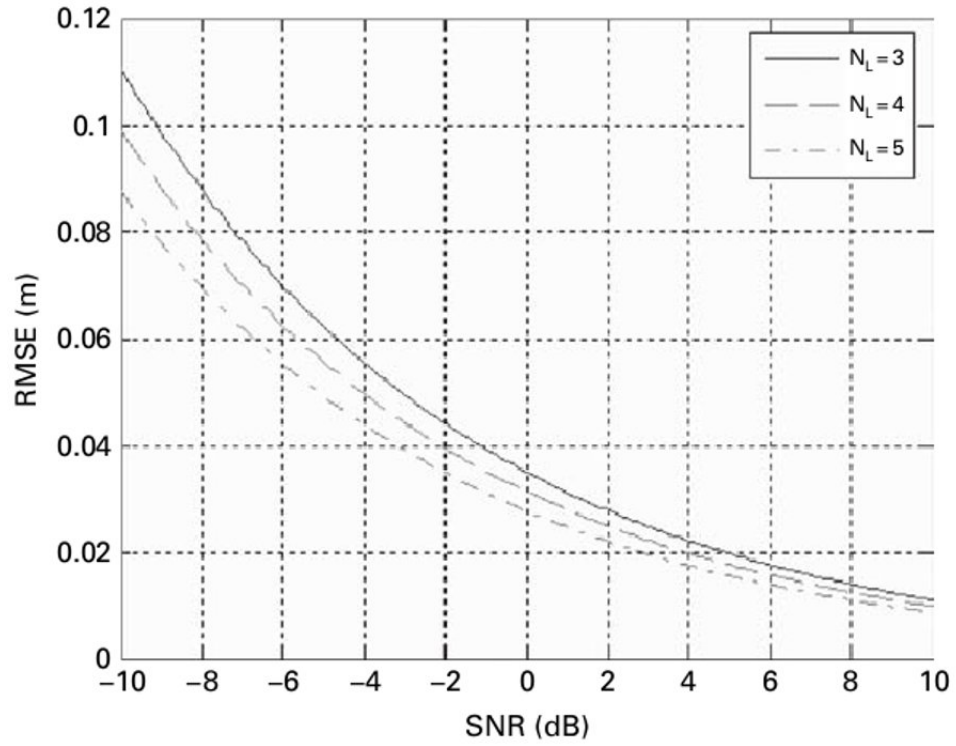
Figure 2.16: Example positioning scenario (from [28]).

Chapter 3

Kalman filter and tracking

In the previous section we discussed statistical positioning using some parameters like TOA and AOA extracted from the received signal at the source nodes. In chapter two we saw that the accuracy of this approach is heavily dependent on the number of LOS source nodes. In practice, indoor positioning has to consider moving obstacles, so we can not be sure to have an ample number of LOS source nodes. Consequently, the accuracy of an indoor positioning system based solely on statistical approaches may be inadequate. In this section we discuss an error mitigation technique to increase the accuracy of an indoor positioning system in practical conditions. The main idea is to use information of previously estimated positions of the target node to estimate its new position with more accuracy.

3.1 Discrete Kalman filter

Kalman filter estimates the new state of a process in two steps. In the first step, prediction, the new state of the process is estimated by previous information in the absence of a new measurement. The second step, correction, uses new noisy measurement as a feedback for correcting estimated value at the prediction step.

3.1.1 Process model

Kalman filter describes the process using two linear models. The first model, called the transition model, represents the relation between the new state and the previous state in the presence of optional control commands and transition noise. The transition model is expressed as

$$\mathbf{x_k} = \mathbf{A}\mathbf{x_{k-1}} + \mathbf{B}\mathbf{u_k} + \mathbf{w_k} \tag{3.1}$$

where $\mathbf{x_k}$ is the state matrix of the process in the kth time interval. For example, the state matrix may include the position of a target node in two dimensions. Matrix $\mathbf{A}$ describes the relation of two successive states in absence of the control command and transition noise. $\mathbf{u_k}$ is the optional control command of the system in the kth time interval and $\mathbf{B}$ describes the effect of control commands on the state. Finally, $\mathbf{w_K}$ is a zero mean white Gaussian noise

with covariance $\mathbf{Q}$. The second model, called the observation model, describes the relation between the measurement and the new state as

$$\mathbf{z_k} = \mathbf{H}\mathbf{x_k} + \mathbf{v_k} \tag{3.2}$$

where $\mathbf{z_k}$ is the noisy measurement vector in the kth time interval, $\mathbf{H}$ describes the relation between state and measurement in absence of the noise and $\mathbf{v_k}$ is the measurement noise which is assumed to be zero mean white Gaussian noise with covariance $\mathbf{R}$.

Note two essential assumptions of the Kalman filter : 1- There are two linear relations which describe the state transitions and the observation vectors. 2- The transition noise and measurement noise are zero mean white Gaussian,

3.1.2   Discrete Kalman filter equations

Kalman filter has two steps discussed formerly; prediction and correction. The prediction step gives an a priori estimate of the new state, $\hat{\mathbf{x}}_\mathbf{k}^-$, based on infromation prior to the kth measurement. Prediction step is represented as (adapted from [26]):

$$\hat{\mathbf{x}}_\mathbf{k}^- = \mathbf{A}\hat{\mathbf{x}}_{\mathbf{k-1}} + \mathbf{B}\mathbf{u_k} \tag{3.3}$$

where $\hat{\mathbf{x}}_{\mathbf{k-1}}$ is the final estimate (posteriory estimate) at $k-1th$ time interval. In the correction step a posteriory estimate is computed as

$$\hat{\mathbf{x}}_\mathbf{k} = \hat{\mathbf{x}}_\mathbf{k}^- + \mathbf{M_k}(\mathbf{z_k} - \mathbf{H}\hat{\mathbf{x}}_\mathbf{k}^-) \tag{3.4}$$

where

$$\mathbf{M_k} = \mathbf{P_k^-}\mathbf{H^T}(\mathbf{H}\mathbf{P_K^-}\mathbf{H^T} + \mathbf{R})^{-1} \tag{3.5}$$

$$\mathbf{P_k^-} = \mathbf{A}\mathbf{P_{k-1}}\mathbf{A^T} + \mathbf{Q} \tag{3.6}$$

$$\mathbf{P_k} = (\mathbf{1} - \mathbf{M_k}\mathbf{H})\mathbf{P_k^-} \tag{3.7}$$

A good intrudction to Kalman filter including more details is given in [26]. A useful observation from equation (3.4) is that the a posteriori estimate is the addition of the a priori estimate and a weighted difference between the measurement and predicted measurement. Note that in equation (3.5) for M_k we observe that if the measurement error $\mathbf{R}$ approaches zero, M_k becomes $\mathbf{H^{-1}}$, and the a posteriori estimate, $\hat{\mathbf{X}}_\mathbf{k}$, is $\mathbf{H^{-1}}\mathbf{z_k}$. In other words, due to the high accuracy of the measurement, we do not use the a priori estimate. On the other hand, if $\mathbf{R}$ becomes significantly larger, M_k approaches zero and the a posteriori estimate is equal to the a priori estimate. In this case, due to large measurement noise we do not trust the new measurement and just use a prior information. We give an example (from [28]) to illustrate the usability of the kalman filter. Assume that there are four source nodes measuring the TOA of a target node which moves with a constant velocity of $1m/s$. Each source node makes four measurements per second. The noise of measurement is modeled by a zero mean normal distribution with variance of $0.5m^2$. At each measurement position

of the target node is estimated by ML algorithm represented by equation (2.36). In this kalman filter the state vector is

$$\mathbf{x_k} = [x_k, y_k, \dot{x}_k, \dot{y}_k] \tag{3.8}$$

where (x_k, y_k) and $(\dot{x}_k, \dot{y}_k)$ are the position of the target node and its velocity at the kth measurement. Also the measurement vector is the output of the ML estimator represented as:

$$\mathbf{z_k} = [x_{z_k}, y_{z_k}]^T \tag{3.9}$$

The matrix $\mathbf{A}$ in equation (3.1) is

$$\mathbf{A} = \begin{pmatrix} 1 & 0 & \Delta t & 0 \\ 0 & 1 & 0 & \Delta t \\ 0 & 0 & 1 & 0 \\ 0 & 0 & 0 & 1 \end{pmatrix} \tag{3.10}$$

where Δt is the time interval between successive measurements. This definition for matrix $\mathbf{A}$ is based on the assumption that the target node is moving with a constant speed; so, for example, our estimate for the new position of the target node and its velocity in the x dimension are

$$\hat{x}_k = x_{k-1} + \Delta t \dot{x}_{k-1} \tag{3.11}$$

and

$$\hat{\dot{x}}_k = \dot{x}_k \tag{3.12}$$

respectively. The noise matrix in the transition model, equation (3.4) is

$$\mathbf{W_k} = \begin{pmatrix} \mathcal{N}(0,0) \\ \mathcal{N}(0,0) \\ \mathcal{N}(0,(\Delta t)^2) \\ \mathcal{N}(0,(\Delta t)^2) \end{pmatrix} \tag{3.13}$$

which applies a random acceleration in order to compensate possible changes of the target node's speed in practice.

Matrix $\mathbf{H}$ in the equation (3.4) is

$$\mathbf{H} = \begin{pmatrix} 1 & 0 & 0 & 0 \\ 0 & 1 & 0 & 0 \end{pmatrix} \tag{3.14}$$

note that our the measurement includes just the position but not the velocity of the target node. Matrix $\mathbf{v_k}$, noise of the measurement, is

$$\mathbf{v_k} = \begin{pmatrix} \mathcal{N}(0,0.5) \\ \mathcal{N}(0,0.5) \end{pmatrix} \tag{3.15}$$

which applies a zero mean normal random noise with $0.5m^2$ variance to the position measurement. Figure 3.1 depicts the probability distribution of the measurement noise for each of the dimensions.
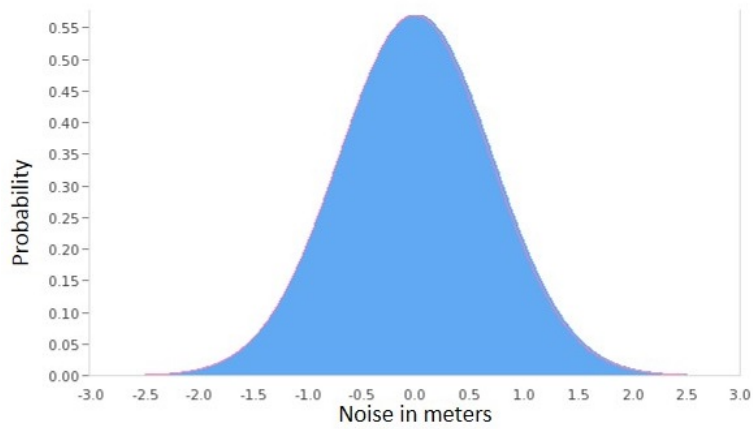
Figure 3.1: Probability distribution of the measuerement noise.

Figure 3.2 depicts the result of this example. The black line is the true path of the target node, crosses are positions estimated by ML and the heavy solid line is the result of applying the kalman filter.
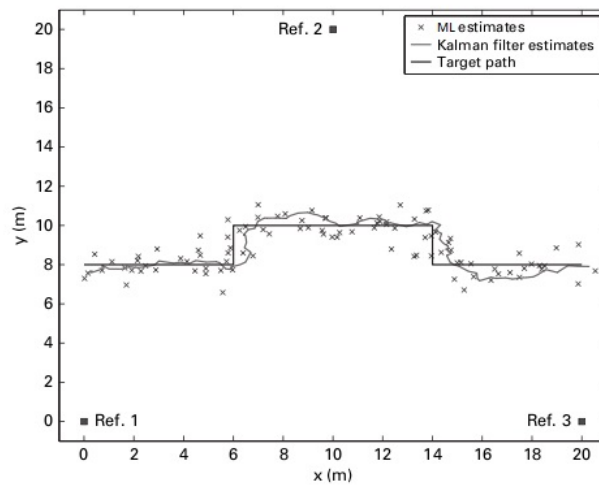
Figure 3.2: Kalman filter example (from [28]).

Chapter 4

Using IEEE 802.15.4a for range estimate

Range estimation gives an estimate of the distance between two nodes.Ranging protocols are based on TOA which is discussed in detail in chapter 2. TOA gives us the time of arrival of the signal at the source node. To compute the range between the target node and the source node we need to know the departure time of the signal. Then the distance is computed by multiplying the time of flight (TOF) by the speed of light. Ranging protocols extract the TOF by different methods. The IEEE 802.15.4a is the first international standard that provides a specific physical layer capable of wireless ranging. IEEE 802.15.4a standard has two formats of communication signal; the first one is impulse radio ultra wide-band (IR-UWB) signals and the second one is chirp spread spectrum (CSS) signals. The second one, CSS, is suitable for data communication purposes while the IR-UWB has the capability of precise ranging. In this chapter we consider the IR signal format.

4.1 IEEE 802.15.4a packet structure

In this section we give a brief overview of packet structure of the IEEE 802.15.4a standard. Figure 4.1 depicts different parts of the packet which is explained in next subsections.

Figure 4.1: IEEE 802.15.4a packet (from [28]).

4.1.1 Preamble

The network protocols preamble is used to synchronize entities with informing arrival of a packet. In IEEE 802.15.4a, the length of the preamble is on of 16, 64, 1024 or 4096 symbols. The symbols used in the preamble part of a packet is one of the eight symbols cited in table 4.1.
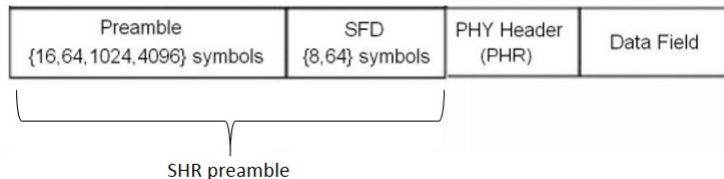
Table 4.1: Different choices for the symbols comprising the preamble.

Index	Symbol
1	-1000010-1011101-10001-111100-110-100
2	0101-10101000-1110-11-1-1-10010011000
3	-11011000-11-11100110100-10000-1010-1
4	00001-100-100-1111101-1100010-10110-1
5	-101-100111-11000-1101110-1010000-00
6	1100100-1-1-11-1011-10001010-11010000
7	100001-101010010001011-1-1-10-1100-11
8	0100-10-10110000-1-1100-11011-1110100

The symbols in 4.1 all have an important property, called perfect periodic auto-correlation, which reduce the error in ranging caused by multipath propagation. The details of this property are out of the scope of this report and is given in [28]. The length of the preamble is chosen regarding the positioning system demands and performance. For example, a larger packet size helps low quality receivers to gain higher SNRs while a smaller packet size reduces the channel occupancy. Lower channel occupancy leads to more efficient energy consumption, and capability of more devices using the same channel. The IEEE 802.15.4a standard includes a parameter, called figure of merit (FOM), which represents the accuracy of the range measurement. It is suggested by the standard [20] for positioning systems to start with the length of 1024 and then adjust the length of the preamble by keeping track of the FOMs.

4.1.2 start of frame delimiter (SFD)

The SDF is a short sequence with 8 or 64 symbols which signals the end of the preamble and start the of the physical layer header. In the ranging protocols the arrival time of the signal and the process time between arrival and sending back an ACK packet should be measured precisely. The SDF is a narrow to trigger starting and stopping of time counting which is necessary for a precise timing.

4.2 Ranging protocols on IEEE 802.15.4a

IEEE 802.15.4a has three different ranging protocols. The basic mandatory protocol is two way time of arrival (TW-TOA). The second one, which is more precise and optional, is

the symmetric double sided (SDS) TW-TOA. The third protocol, called private ranging, is designed for systems in which the position information is sensitive and should be kept private. These three ranging protocols are discussed in the next subsections respectively.

4.2.1 TW-TOA protocol

In the pure TOA system, the target node reports the departure time of the signal; hence the source node is able to compute the TOF of the signal. This TOA approach dedicates a necessary synchronization between the target node and the source node; since the departure time is measured by the target node and is used by the source node. The main advantage of TW-TOA over the TOA approach is its independence from the synchronization. Figure 4.2 depicts the TW-TOA protocol. The TW-TOA protocol consists of the following steps:

1. The target node sends a ranging request, $RFRAME_{req}$, to the source node, and records the departure time of the frame, T_1.

2. The source node replies to the ranging request after arrival with the $RFRAME_{rep}$.

3. The target node records the arrival time of the $RFRAME_{rep}$, T_2.

The target node computes the round-trip time T_r as

$$T_r = T_2 - T_1 \tag{4.1}$$

and then the TOF between the target node and the source node, called T_{TW}, is given by

$$T_{TW} = T_r/2 \tag{4.2}$$

and the distance between two nodes is given by

$$d = cT_{TW} \tag{4.3}$$

where c is the speed of light. With three distances from three source nodes, the target node can determine its position based on the known positions of the source nodes. In practice, as is depicted in Figure 4.2, there is a delay on the source node side between receiving of the $RFRAME_{req}$ and sending $RFRAME_{rep}$ called the turn around time T_{ta}^B. Due to the high speed of the light, a T_{ta}^B of nano-seconds causes a ranging error of tens of centimeters. Consequently, it is important to have an accurate estimate of the T_{ta}^B.
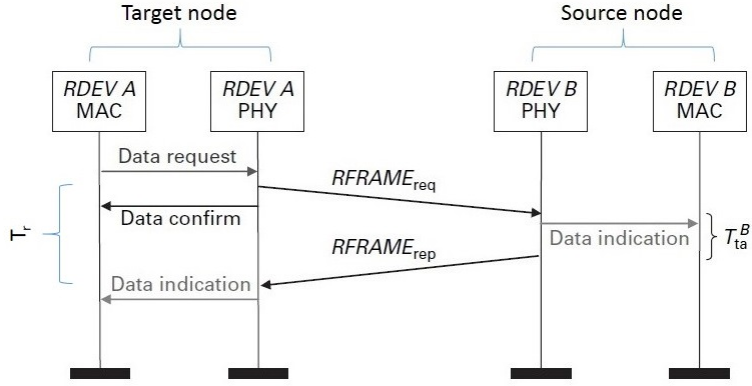
Figure 4.2: TW-TOA ranging protocol (from [28]).

IEEE 802.15.4a uses a more advanced TW-TOA approach which gives an estimate of the T_{ta} to the target node for more accurate ranging. Figure 4.3 depicts this approach. A counter in the source node starts when detecting the first symbol of the SFD of $RFRAME_{req}$ and stops when the first symbol of SFD in $RFRAME_{rep}$ is sent. Then, after sending $RFRAME_{rep}$, the source node sends a time stamp report including the stop and start value of the counter. Finally, the target node sends an ACK back to the source node. Using this approach, the TOF is computed as

$$T_{TW} = \frac{T_r - T_{ta}^B}{2} \tag{4.4}$$
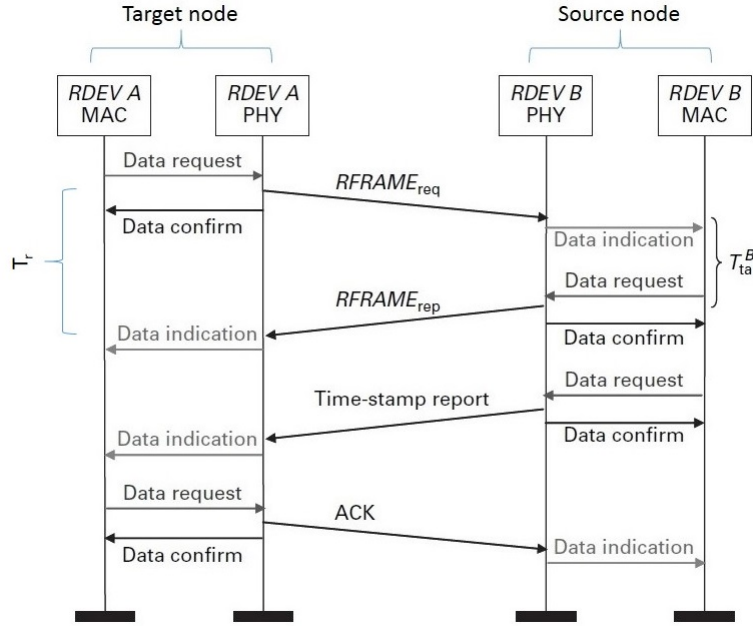
Figure 4.3: More accurate TW-TOA (from [28]).

4.2.2 SDS-TW-TOA protocol

One of the error sources in the TW-TOA approach is the clock offset. The crystal oscillators used in sensor devices (source or target nodes) are not working exactly with the nominal frequency, so there is a small positive or negative offset in the time measurements. with the high speed of light, this small offset may cause a significant error in ranging. The SDS protocol is designed to mitigate the clock offset error. In the SDS protocol, depicted in Figure 4.4, after the target node receives the $RFRAME_{rep}$, it sends a second $RFRAME_{req}$ to the source node. Consequently, each of the nodes has an estimate of the round trip time, T_r, and turn around time, T_{ta}. Finally, the source node sends a time stamp including measured T_r and T_{ta} to the target node.
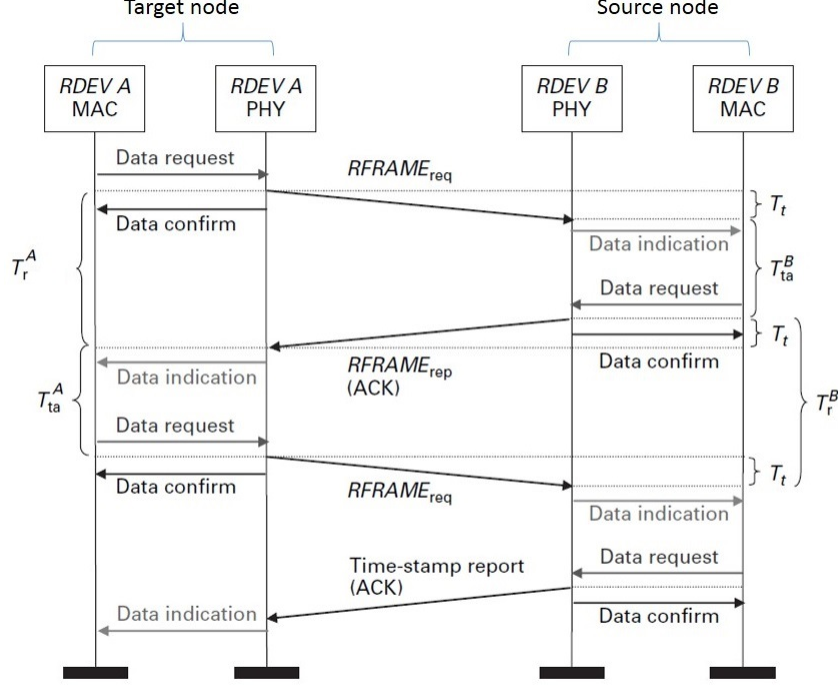
Figure 4.4: SDS ranging protocol (from [28]).

Then the target node estimates the TOF as

$$T_{SDS} = \frac{(T_r^A - T_{ta}^A) + (T_r^B - T_{ta}^B)}{4} \tag{4.5}$$

To observe the merit of the SDS protocol over the TW-TOA protocol, we define the frequency offsets of the target node and source node e_A and e_B as

$$e_A = \frac{Rf_A - Nf_A}{Nf_A} \tag{4.6}$$

$$e_B = \frac{Rf_B - Nf_B}{Nf_B} \tag{4.7}$$

where Rf_x and Nf_x are the real frequency and nominal frequency of the node x. Then estimates of the TOF given by the TW-TOA protocol and the SDS protocol are represented as

$$\hat{T}_{TW} = \frac{T_r^A(1 + e_A) - T_{ta}^B(1 + e_B)}{2} \tag{4.8}$$

$$\hat{T}_{SDS} = \frac{(T_r^A - T_{ta}^A)(1 + e_A) + (T_r^B - T_{ta}^B)(1 + e_B)}{4} \tag{4.9}$$

37

Note that in the indoor positioning systems, measured distances are not much more than 30 meters, therefore the maximum of T_{TW} and T_{SDS}, which are the time it takes for light to travel about 30 meters, are in the order of $0.1\mu s$. Another point is that the T_{ta} is not just the response time of the device but also includes the duration of packet, and is on the order of milliseconds. Consequently, T_{TW} and T_{SDS} are much smaller than T_{ta}. The error of each estimation is represented as

$$\hat{T}_{TW} - T_{TW} = T_{TW}e_A + \frac{e_A - e_B}{2}T_{ta}^B \tag{4.10}$$

$$T_{TW} \ll T_{ta}^B \Rightarrow \hat{T}_{TW} - T_{TW} \approx \frac{e_A - e_B}{2}T_{ta}^B \tag{4.11}$$

$$\hat{T}_{SDS} - T_{SDS} = \frac{T_{SDS}}{2}(e_A + e_B) + \frac{T_{ta}^B - T_{ta}^A}{4}(e_A - e_B) \tag{4.12}$$

$$T_{SDS} \ll T_{ta}^B - T_{ta}^A \Rightarrow \hat{T}_{SDS} - T_{SDS} = \frac{T_{ta}^B - T_{ta}^A}{4}(e_A - e_B) \tag{4.13}$$

We observe that the clock offset error is mitigated in the SDS protocol since the T_{ta}^B is significantly larger than $T_{ta}^B - T_{ta}^A$. Tables 4.2 and 4.3 show some typical results for the frequency offset error computed by equation (4.11) and (4.13). We see that the SDS protocol mitigates the frequency offset error significantly.

Table 4.2: Frequency offset error using the TW-TOA protocol (from [1]).

T_{ta}^B	$e_A - e_B$			
	2ppm	20ppm	40ppm	80ppm
$100\mu s$	0.1 ns	1 ns	2 ns	4 ns
5ms	5 ns	50 ns	100 ns	200 ns

Table 4.3: Frequency offset error using the SDS protocol (from [1]).

$T_{ta}^B - T_{ta}^A$	$e_A - e_B$			
	2ppm	20ppm	40ppm	80ppm
$1\mu s$	0.0005 ns	0.005 ns	0.01 ns	0.02 ns
$10\mu s$	0.005 ns	0.05 ns	0.1 ns	0.2 ns
$100\mu s$	0.05 ns	0.5 ns	1 ns	2 ns

4.2.3 Private ranging protocol

In some cases the ranging information is sensitive. A hacker may perform different attacks. He may just eavesdrop to determine the range and consequently position information. He may also try to disturb the ranging protocol by sending a fake response. The IEEE802.15.4a

standard has an optional private ranging protocol which provides some security services. The first technique used in the private ranging protocol is encrypting the time stamps before sending them. The rational of this technique is that having all information but the time stamp the hostile is not able to compute the range between two nodes. Note that this encryption is performed before sending the time stamp and after time measurements so it is not time sensitive. The second method used in the private ranging protocol is dynamic preamble selection (DPS). Through this approach, ranging nodes use a longer preamble with 127 symbols. The source node and the target node agree on the preamble sequence, among eight different choices, by passing encrypted messages in the beginning of the ranging protocol. The preambles must change for each ranging process to protect the system against reply attacks.

Chapter 5

Commercial UWB positioning devices

There are several devices in the market produced to use in positioning systems. Our focus is on those which use UWB technology and specially,are compliant with IEEE802.15.4a standard. Following we discuss some of these devices with explaining their advantages and disadvantages.

5.1 Ubisense technology

The Series 9000 IP sensors of Ubisense company use UWB technology to determine the position of the Tags (target nodes) in real time. The most important feature of this device is that it has an array of antennas instead of a single antenna. This feature gives the ability of using AOA approach in positioning to the Ubisense sensors. As discussed in the second chapter, manipulating the AOA approaches, positioning system is able to work with fewer number of sensors. In other words, the position of the target node is determined just if it is detected by two sensors while without using of the AOA approach, we need three sensors detecting the target node at least. This feature may cause a significant difference in cost of a large indoor positioning system. Ubisense sensor's dimension is $20 \times 14 \times 6.5$ cm for the smallest option and its weight is 580 g. The company claims that the accuracy of the positioning sensor is 15 cm. These sensors are able to communicate with each other over wired or wireless connection and the update frequency for positioning is up to 134 Hz. Ubisense provides an academic research packages which includes 4 stationary sensors, 10 tags, needed software and support. The price of this package is 12,500 USD. The Ubisense sensor, to our knowledge, is not programmable for research and development. It is, however, a good choice for industrial purposes since it has a solid cover, good communication facilities and AOA measurement.

Figure 5.1: Ubisense real time location technology (from the Ubisense website : www.ubisense.net/).

5.2 Time Domain technology

Time Domain is another company researching and developing in the field of real time positioning with UWB signals. P410 is the name of their released product for ultra wideband ranging and communication. This module is capable of two ranging methods, two way time of flight (TW-TOF) and coarse rang estimation (CRE). CRE method estimates the range by the signal strength and is calibrated by TW-TOF with specific intervals. The accuracy of the CRE is less than accuracy of the TW-TOF but its update frequency is higher. P410 can connect to two antennas simultaneously; hereby it can acts as a radar. As cited in the brochure, the accuracy of the P410 is 2 cm in the LOS condition and 10 cm in the combined NLOS condition. This module is programmable and has USB interface. The module dimension is $7.6 \times 8 \times 1.6$, the measurement range is up to 354 m and the update rate is up to 153.8 Hz.The center frequency is 4.3 GHz and the bandwidth is 2.2 GHz. This module has some really interesting specification such as its accuracy, however, this technology doesn't provide a small, low power and less expensive tag for moving nodes. So all of the nodes including the target node have to use the main 4.2 W module with above dimension. Time Domain provides a Devkit which includes 4 P410 modules with their antennas and power supplies, needed software and 5 hours of support; the price of devkit is 9,995 USD and each extra P410 module costs 1,995 USD.

Figure 5.2: Time Domain real time location technology (P410) (from the Time Domain website : www.timedomain.com/).

5.3 Decawave technology

The Decawave company has a IEEE802.15.4a compliant sensor which is able to perform positioning by TOA or TDOA approaches. The producer claims that the accuracy of this sensor working with 1.3GHz bandwidth is $+/-10$ cm. According to the producer website, the key benefits of this sensor, called DW1000, are precise ranging, long LOS and NLOS communication range (up to 290m), high data rate (up to 6.8 Mbit/s) and low power consumption. The EVB1000 Evaluation Board is a complete device including the DW1000 IC, ARM programmable processor, LCD, USB connection and antenna. The dimensions of the EVB1000 is 7×7 cm excluding the off-board antenna and the range of the center frequency of six available UWB channels is 3.5 to 6.5 GHz. The Decawave's device is more suitable for research and development because it is programmable and smaller and it has embedded LCD and USB connections. The price of the evaluation kit is 606.67 USD, the price of the module which includes transmitter IC and integrated antenna is about 30 USD and the price of a single transmitter IC is 14.75 USD.

Figure 5.3: Decawave real time location technology (from the Decawave website : www.decawave.com/).

5.4   Zebra technology

The Dart UWB transceiver is a product of the Zebra company. Dart technology provides positioning with 30 cm precision. The most important feature of the Dart technology is its small circular tags, 4 cm in diameter, which include an embedded battery for up to 7 years of life depending on the duty cycle. These tags are compliant with 802.15.4f, an amendment of 802.15.4a which specifies PHYs for UWB RFIDs. The range for this technology is up to 200 m. The Dart technology includes the Dart Hub, Dart Sensors and Dart Tag. The positioning software is implemented on the Dart Hub. In addition, the Dart Hub provides power, data and clock for the Dart Sensors. The Dart Sensors act as source nodes to receive the UWB from the Dart tags which are attached to moving objects. The positioning approach used in Dart technology is TDOA. The price of the Zebra demo kit which includes tags and needed infrastructure is about 12,000 USD.

Figure 5.4: Zebra Dart UWB real time location technology (from the Zebra website : www.zebracanada.com/).

5.5   Nanotron technology

Nanotron is another company researching and producing in the field of the real time location. It offers a positioning infrastructure including the anchors (source nodes) and the tags (target nodes). Two good features of their technology are a LiPo embedded battery for the tags and adjustable signal power. The main drawback of the Nanotron technology is that uses the chirp spread spectrum physical layer technology instead of using the impulse radio; that is why the accuracy of their technology is significantly weaker in comparison with Ubisense and Decawave. The Nanotron real time location (RTL) technology's accuracy is 1 m to 3 m. The positioning approach used Nanotron is TDOA. Nanotron provides a test kit which includes 8 stationary nodes, 5 tags and needed software. The price of this package with educational discount is 3,833.50 EUR.

Figure 5.5: Nanotron real time location technology (from the Nanotron website : www.nanotron.com/).

5.6 Apple's iBeacon

Apple offers a new technology, called iBeacon, which is able to detect iOS or Android devices near a stationary transceiver. The majority of applications of this technology are in marketing; for example customers can receive the list of sale items in a local store and they can also pay at the checkout counter without taking wallet out (see [13]). iBeacon works on bluetooth low energy (BLE) wireless communication and uses narrow bound wireless signals. Consequently it cannot provide precise positioning as UWB can. iBeacon stationary nodes can identify devices by their proximity in one of three classes:

- Immediate : Devices within 10 cm or less

- Near : Devices around 2 to 3 m away

- Far : Devices between 3 m and 70 m away

The above ranging satisfies for the goals of iBeacon technology but this accuracy is far from UWB technologies and is not usable in real time location systems.

5.6.1 Summary

Table 5.1 gives a general comparison between the three UWB positioning systems cited in this chapter.

Table 5.1: Comparison between three different UWB positioning systems.

System	Estimated LOS Accuracy	Range update rate	Range	Size	Technology	IEEE 802.15.4a compliant
Decawave	10cm	NA	290m	7 × 7cm (Evaluation Board)	IR-TOA and TDOA	Yes
Ubisense	15cm	up to 134Hz	NA	20×14×6.5 (Stationary node)	IR-AOA and TDOA	No
Time Domain	2cm	up to 153.8Hz	up to 354	7.6×8×1.6	IR-TW-TOF and CRE	No
Zebra	30cm	up to 200Hz	up to 200m	4cm diameter	TDOA	No (802.15.4f)
Nanotron	1-3m	up to 100Hz	50m	11.9×9.8×1.8 cm (Stationary node)	CSS-TDOA	No

System	Bandwidth	Price
Decawave	900 MHz	606.67 USD for evaluation kit and 14.75 USD for IC
Ubisense	NA	12500 USD for 4 stationary and 10 tags
Time Domain	2.2 GHz	9995 USD for 4 modules plus accessories
Zebra	NA	12000 USD for tags and infrastructure
Nanotron	80 MHz	3,833.50 EUR for 8 stationary nodes and 5 tags

Chapter 6

Summary and future work

6.0.2 Summary

In this report we presented an introduction to the real time positioning of target nodes by use of UWB signals. We started with the definition and important features of UWB signals in chapter 1. In chapter 2, we discussed four approaches (RSS, TOA, TDOA, AOA) for wireless positioning and the suitability of UWB signals for precise wireless positioning. In addition, we considered the presence of noise and presented statistical approaches to mitigate positioning error in practice. Kalman filtering is a common technique used for increasing the accuracy of dynamic positioning systems. Kalman filtering is discussed briefly in chapter 3. The IEEE802.15.4 international standard defines a physical and MAC layer for devices implementing UWB positioning. We introduced the IEEE802.15.4 standard and its three ranging protocols in chapter 4. Chapter 5 gives an introduction to four commercial devices available for the UWB real-time positioning. Khodjaev et al [14] present a good survey on NLOS detection and NLOS error mitigation algorithms.

6.0.3 Future work

The main error source of UWB positioning systems is NLOS communication; for example concrete walls which are fairly common in modern buildings decrease the accuracy of positioning systems significantly. Consequently, in many NLOS environments the positioning error is much more than the error in LOS condition and on the order of meters. There are several approaches to overcome this problem.

The first approach is to detect NLOS measurements and try to mitigate NLOS errors in these measurements or simply eliminate them. There are many papers which introduce different methods for this approach. Wann et al [25] introduced a biased Kalman filter to mitigate the NLOS error. They use the standard deviation and a couple of previous signals to detect a NLOS signal. Guvenc et al [10] introduce another method for detection and mitigating of the NLOS error based on channel statistics such as kurtosis. Gao et al [8] suggest a learning algorithm which uses particle swarm to identify and mitigate the NLOS error.

The second approach is to reduce the cost of covering all of the indoor rooms by LOS source nodes. With the straight-forward positioning approaches like those we discussed in section 2.1, we need at least three source nodes to determine the three dimensional position of the target node. If we want to cover all the indoor rooms with LOS source nodes we need $3R$ of source node devices, where R is the number of rooms. Some combined approach such as AOA/TDOA (see [27] for details) are able to perform three dimensional positioning with only two source nodes which reduces the cost of needed infrastructure. Note that AOA source nodes need an array of antennae (at least two antennas) which makes this device more complex than other source nodes (such as TOA source nodes). Another idea to reduce the number of needed nodes is to connect more than one antenna to a single source node device (UWB receiver). If we connect three antennas to a receiver and switch between these three antennas respectively, we are able to obtain the TOA of the signal from three different known positions (position of the antennas). Consequently we determine the three dimensional position of the target node with a single UWB receiver. This approach decreases the cost of positioning infrastructure to one third of the original amount. Although this approach is less expensive, it reduces the update rate of positioning. It can be shown that with high update rate of the commercially available devices and average speed of walking or even running of humans or robots, the update rate remains satisfactory. Having an ultra wide-band channel for transmitting the unfiltered signal from the antenna to the receiver is another challenge of this approach. Galler et al [7] have provided an approach using two antennas to obtain an AOA/TOA measurement and determine the two dimensional position of the target node with a single receiver.

Inertial navigation systems (INS) are a family of navigation systems which use motion and rotation sensors (accelerometers and gyroscopes) to determine the position of a moving node. The major problem with INS systems is that they lose accuracy with the passage of time. The third approach to increase the accuracy of positioning in NLOS situation is coupling the INS and the UWB positioning system. It is declared [3] [29] [6] [11] that these two systems are able to cover the drawbacks of each other and gain a better result.

Bibliography

[1] IEEE standard for information technology - telecommunications and information exchange between systems - local and metropolitan area networks - specific requirement part 15.4: Wireless medium access control (mac) and physical layer (phy) specifications for low-rate wireless personal area networks (wpans). *IEEE Std 802.15.4a-2007 (Amendment to IEEE Std 802.15.4-2006)*, pages 1–203, 2007.

[2] S. Al-Jazzar and J. J. Caffery. Ml and bayesian toa location estimators for nlos environments. *IEEE Veh. Technol. Conf. (VTC)*, 2:11781181, 2002.

[3] C. Ascher, L. Zwirello, T. Zwick, and G. Trommer. Integrity monitoring for uwb/ins tightly coupled pedestrian indoor scenarios. In *Indoor Positioning and Indoor Navigation (IPIN), 2011 International Conference on*, pages 1–6. IEEE, 2011.

[4] F. C. Commission. First report and order 02-48, part 15 (radio frequency devices), subpart f (ultra-wideband operation) (last visited : 19.11.2013). Feb. 2002.

[5] L. Cong and W. Zhuang. Hybrid toa/aoa mobile user location for wideband cdma cellular systems. *IEEE Trans. Wireless Commun*, 1(3):439447, 2002.

[6] A. De Angelis, J. Nilsson, I. Skog, P. Händel, and P. Carbone. Indoor positioning by ultrawide band radio aided inertial navigation. *Metrology and Measurement Systems*, 17(3):447–460, 2010.

[7] S. Galler, W. Gerok, J. Schroeder, K. Kyamakya, and T. Kaiser. Combined aoa/toa uwb localization. In *Communications and Information Technologies, 2007. ISCIT '07. International Symposium on*, pages 1049–1053, Oct 2007.

[8] W. Gao, K. Veeramachaneni, G. Kamath, and L. Osadciw. A novel ultrawide band locationing system using swarm enabled learning approaches. In *Swarm Intelligence Symposium, 2009. SIS'09. IEEE*, pages 129–136. IEEE, 2009.

[9] A. Gut. *IntermediateCourse*. Springer-Verlag, 1995.

[10] I. Guvenc, C.-C. Chong, and F. Watanabe. Nlos identification and mitigation for uwb localization systems. In *Wireless Communications and Networking Conference, 2007. WCNC 2007. IEEE*, pages 1571–1576. IEEE, 2007.

[11] E. P. Herrera, R. Quirós, and H. Kaufmann. Analysis of a kalman approach for a pedestrian positioning system in indoor environments. In *Euro-Par 2007 Parallel Processing*, pages 931–940. Springer, 2007.

[12] J. J. C. Jr. *Wireless Location in CDMA Cellular Radio Systems*. 2000.

[13] H. D. T. H. S. M. KHAN Ahmer A, Tucker Brian J. Method to send payment data through various air interfaces without compromising user data. PATENT, January 2014.

[14] J. Khodjaev, Y. Park, and A. S. Malik. Survey of nlos identification and error mitigation problems in uwb-based positioning algorithms for dense environments. *annals of telecommunications-annales des télécommunications*, 65(5-6):301–311, 2010.

[15] W. Kim, J.-G. Lee, and G.-I. Jee. The interior-point method for an optimal treatment of bias in trilateration location. *Vehicular Technology, IEEE Transactions on*, 55(4):1291–1301, 2006.

[16] H. V. Poor. *An Introduction to Signal Detection and Estimation*. New York: Springer-Verlag, 1994.

[17] Y. Qi. *Wireless geolocation in a non-line-of-sight environment*. PhD thesis, Princeton University, 2003.

[18] Y. Qi, H. Kobayashi, and H. Suda. Analysis of wireless geolocation in a non-line-of-sight environment. *Wireless Communications, IEEE Transactions on*, 5(3):672–681, 2006.

[19] R. I. Reza. *Data fusion for improved TOA/TDOA position determination in wireless systems*. PhD thesis, Virginia Tech, 2000.

[20] Z. Sahinoglu and S. Gezici. Ranging in the ieee 802.15.4a standard. In *Wireless and Microwave Technology Conference, 2006. WAMICON '06. IEEE Annual*, pages 1–5, 2006.

[21] A. Sayed, A. Tarighat, and N. Khajehnouri. Network-based wireless location: challenges faced in developing techniques for accurate wireless location information. *Signal Processing Magazine, IEEE*, 22(4):24–40, 2005.

[22] S. Schwartz and J. Bobier. Going beyond interruptible usage.

[23] C. E. Shannon. Communication in the presence of noise. *Proc. Institute of Radio Engineers*, 1(37):10–21, 1949.

[24] B. R. J. Sichun Wang, Robert Inkol. Relationship between the maximum likelihood emitter location estimators based on received signal strength (rss) and received signal strength difference (rssd). In *26th Biennial Symposium on Communications (QBSC)*, pages 503–513, 2012.

[25] C.-D. Wann and C.-S. Hsueh. Nlos mitigation with biased kalman filters for range estimation in uwb systems. In *TENCON 2007-2007 IEEE Region 10 Conference*, pages 1–4. IEEE, 2007.

[26] G. Welch and G. Bishop. An introduction to the kalman filter. *University of North Carolina at Chapel Hill, Chapel Hill, NC*, 7(1), 1995.

[27] C. Yang, Y. Huang, and X. Zhu. Hybrid tdoa/aoa method for indoor positioning systems. In *Location Technologies, 2007. The Institution of Engineering and Technology Seminar on*, pages 1–5. IET, 2007.

[28] I. G. Zafer Sahinoglu, Sinan Gezici. *Ultra-wideband Positioning Systems: Theoretical Limits, Ranging Algorithms, and Protocols*. Cambridge University Press, October 6, 2008.

[29] L. Zwirello, C. Ascher, G. F. Trommer, and T. Zwick. Study on uwb/ins integration techniques. In *Positioning Navigation and Communication (WPNC), 2011 8th Workshop on*, pages 13–17. IEEE, 2011.

[30] L. Zwirello, T. Schipper, M. Harter, and T. Zwick. Uwb localization system for indoor applications: Concept, realization and analysis. *JECE*, 2012:4:1–4:11, Jan. 2012.